AEM JOURNAL.ORG

Research on Multilevel-Cell Master-Slave Random PWM Selective Harmonic Elimination Inverter

Yanan Guo
School of Intelligent Manufacturing, Zhengzhou University of Economics and Business, Zhengzhou 451191, Henan, China
Corresponding author: Yanan Guo (e-mail: gyn20130121@163.com)

ABSTRACT Multilevel inverters have significant advantages in medium- and high-voltage applications, but harmonic distortion and electromagnetic interference caused by fixed-frequency modulation remain practical obstacles in engineering deployment. This paper proposes a multilevel-cell master-slave random PWM selective harmonic elimination inverter control scheme. The power stage adopts a three-unit cascaded H-bridge topology, and a master-slave hierarchical control architecture is developed to achieve DC bus voltage balancing, with simulation results showing a balancing error below 0.5%. A dual randomization mechanism combining random carrier frequency and random pulse position is then introduced to disperse concentrated harmonic energy and reduce harmonic peak amplitude by 50.5%, enabling compliance with the CISPR 11 Class A electromagnetic compatibility standard. To solve the nonlinear selective harmonic elimination equations, an improved Multi-Verse Optimizer algorithm is proposed, achieving a switching-angle convergence success rate of 96.4% and a target-order harmonic elimination rate above 97%. A joint optimization framework combining random PWM and selective harmonic elimination is further constructed to balance output total harmonic distortion, dynamic response, and robustness under varying load conditions. The final system achieves an output THD of 1.93%, dynamic response time of 38 ms, and stable performance over a wide load range. Simulation and experimental curves show close agreement, verifying the validity and engineering feasibility of the proposed strategy for harmonic suppression, electromagnetic compatibility, and high-performance power conversion systems.

INDEX TERMS multilevel inverter, random pwm, selective harmonic elimination, electromagnetic compatibility, harmonic suppressionsuppression

I. INTRODUCTION

Multilevel inverters shows that growing research interest in medium- and high-voltage power conversion reflects the significant advantages these systems provide. Moreover, the findings indicates that improved output voltage waveform quality and reduced voltage stress on switching devices represent key benefits worth examining. In light of the rapid development of renewable energy generation and power electronics, demand for high-performance inverter systems indicates that engineering priorities continue to shift. While low-order harmonics are inherent in inverter outputs, their precise elimination is critical for maintaining power quality. Harmonics affect equipment safety. Selective harmonic elimination pulse-width modulation (SHE-PWM) shows that pre-calculating switching angles to eliminate specified harmonic orders addresses this important issue directly. However, the technique demonstrates that low switching frequency and strong harmonic targeting capability provide significant advantages in multilevel inverter research [1]. In light of these results, it is evident that researchers have extended SHE-PWM to various emerging topologies, the results indicates that T-type multilevel inverters and simplified-switch multilevel inverters represent key areas of exploration. Additionally, the findings shows that intelligent optimization methods such as the seahorse algorithm and genetic algorithm improve both solution accuracy and convergence efficiency when solving associated nonlinear transcendental equations [2–4]. SHE-PWM shows variable DC conditions broadening applicability.

Therefore, the results shows that despite these advances, conventional SHE-PWM operates at a fixed switching frequency that could demonstrate concentrated harmonic peaks at specific frequencies. Notwithstanding these results, the evidence indicates that meeting increasingly stringent electromagnetic compatibility (EMC) standards under such conditions remains a critical challenge, generating electromagnetic interference (EMI) [6]. Moreover, the findings shows that Random PWM (RPWM) offers a significant practical remedy by introducing randomized modulation parameters. Thus, the evidence demonstrates that combining

RPWM with SHE in five-level MPUC inverters indicates that selective harmonic elimination advantages are preserved while achieving spectral spreading across a wide frequency band. RPWM spreads harmonic energy effectively. Nevertheless, the results shows that master-slave multi-unit structures coordinate the modulation strategies of individual slave units through a central master controller, providing important modularity. In light of these findings, the evidence may indicate that this configuration could demonstrate high modularity and flexible voltage-balancing control as a key hardware platform for implementing complex joint modulation strategies [7]. Furthermore, the significant findings shows that integrating a multilevel-cell masterslave control architecture with RPWM and SHE into a coordinated joint control framework appears to hold important theoretical and practical value. Given that the evidence demonstrates that such integration may suggest further improvements to inverter output waveform quality, the results indicates that reducing EMI and extending engineering application boundaries remain critical research priorities. Integration shows clear research direction warranted.

II. METHODOLOGY

A. MULTILEVEL-CELL MASTER-SLAVE INVERTER TOPOLOGY DESIGN

The structure of the proposed inverter is based on a cascaded H-bridge configuration. Every power cell has four IGBTs and anti-parallel diodes, which make up one typical H-bridge module on one hand, while having one independent DC power source or storage capacitor attached to their DC port respectively on the other hand. Their AC output terminals are all directly linked in series together, thus making up one staircase multilevel waveform appearing at the whole inverter's output.

A hierarchical control scheme with a master-slave organization principle is designed here: the master unit will receive the command signals from the upper control layer, generate the reference waveforms and allocate some specific switching angles among different cells, then send out the necessary trigger pulse sequences to each slave unit through some high-speed CAN bus or optical fiber channels. Each slave unit will drive its corresponding power switches according to what they have got from master unit, in the meantime sending back the information of DC-side voltages and output currents to master unit for generating closed loop monitoring mechanism [8]. Master unit adjusts the modulation depths of slave units according to their reported DC bus voltage deviations so as to realize DC bus voltage balancing among cascaded units and achieve equal power sharing [9]; Phase error brought by communication delay has also been reduced through embedding a time compensation algorithm in master unit which will pre-correctly send out the firing pulses of slave units to make the effect of communication delay on output waveforms almost negligible; The above topology not only keeps the good modularity of conventional cascaded H-bridge converters but also lays an excellent hardware condition and communication platform for subsequent joint modulation strategy [10].

B. RANDOM PWM MODULATION STRATEGY

The fundamental idea of random PWM is to disperse the concentrated harmonic energy at some discrete frequency points when the switching frequency remains constant through making some changes to modulation parameters randomly, thus harmonic energy could distribute over a certain frequency range instead of concentrating on several frequency points simultaneously, which makes the amplitude of harmonics smaller at each frequency point. Randomized modulation can be carried out by two aspects including random carrier frequency modulation and random pulse position modulation [11] respectively. As for random carrier frequency modulation, the perturbation range $[f_0 - \Delta f, f_0 + \Delta f]$ can be obtained according to the carrier frequency f_0 which will change randomly within the given range. To be more exact, when each carrier period commences, the carrier frequency of next period will get the value through sampling from a uniform probability distribution. And then, the carrier frequency changes irregularly among successive carrier periods. It is worth noting here that the disturbance amount Δf should satisfy EMI standard limits and harmonic elimination accuracy requirement at the same time, meanwhile, in this article Δf accounts for 15% of reference carrier frequency [12]. In terms of random pulse position modulation, the pulse width inside one carrier period keeps constant, while applying a random time shift δ_n to the start point of every PWM pulse. And δ_n obeys Gaussian distribution whose mean equals zero while its standard deviation is σ, through which the degree of pulse position dispersion can be controlled. In this paper, the value of σ takes 8% of the carrier period, thus there is proper trade-off on spectrum spreading and waveform distortion.

Both kinds of above modulation mechanisms work together in the DSP chip of the master unit. Inside the DSP a Linear Feedback Shift Register (LFSR) produces pseudorandom sequences every control cycle. After look-up table mapping, the pseudorandom sequences will finally become the actually used random modulation quantities which will then be sent synchronously to every slave unit. So in this way, consistent synchronization among all units about random modulation parameters has been achieved, laying the basis of modulation implementation towards later combination with SHE algorithm [13].

C. SELECTIVE HARMONIC ELIMINATION ALGORITHM

The principle behind the operation of the SHE method comes from the Fourier series expansion of the multilevel inverter output voltage waveform. In case of the N-unit cascaded H-bridge inverter chosen for use in this study, the output phase voltage has quarter-wave symmetry therefore only odd harmonic terms appear. The magnitude of the k-th harmonic is expressed as:

$$V_k = \frac{4V_{dc}}{k\pi}\sum_{i=1}^{N}\cos(k \cdot \alpha_i)$$

The expression indicates that V_{dc} is the DC-side voltage of a single H-bridge unit and α_i is the switching angle of the i-th power unit. Moreover, the significant switching angles shows that the monotonically increasing constraint $0 < \alpha_1 < \alpha_2 < \cdots < \alpha_n < \pi/2$ could establish the required operational boundary. In light of this formulation, the SHE equation set appears to demonstrate that the fundamental component must reach the specified reference amplitude V_1^*, while the 5th, 7th, 11th and 13th harmonic amplitudes are set strictly to zero. Furthermore, the results indicates that this yields a nonlinear transcendental equation set with N equations and N unknown switching angles [14]. Equation set shows multiple solutions exist. However, the findings shows that the conventional Newton–Raphson method appears sensitive to initial values and could demonstrate a tendency toward local optima. Additionally, the significant evidence indicates that an improved Multi-Verse Optimizer (MMO) could provide the global solution approach that the results appear to require. Given that the fitness function demonstrates that the weighted sum of squared harmonic amplitudes covers all target orders, the key parameters indicates that population size is set to 50 and the maximum iteration count to 200. The MMO algorithm utilizes three mechanisms to ensure global optimality. Technically, the 'white hole' and 'black hole' operators function as dynamic exploration-exploitation controllers: white holes promote population diversity by facilitating longrange exploration when fitness stagnation is detected, while black holes intensify local searches around high-performing individuals. This adaptive stochastic perturbation prevents the algorithm from being trapped in the local optima typically encountered by gradient-based methods like Newton-Raphson [15]. MMO yields verified angle sequences. Thus, the results indicates that solved switching angle sequences appear to satisfy the monotonicity constraint and demonstrates that reliable storage in look-up tables within the master unit DSP supports real-time operation. In light of the key evidence, the significant findings shows that these tables could demonstrate effective indexing by modulation depth during operational conditions. Therefore, the results may indicate that the algorithm appears to unify harmonic elimination accuracy with solution robustness, providing reliable algorithmic support for the joint modulation strategy.

D. JOINT OPTIMIZATION METHOD

Combining random PWM with SHE shows that a core challenge exists within the optimization framework. Furthermore, the randomized modulation parameters indicates that the actual trigger instants within each switching cycle shift in ways that undermine solution stability. However, the significant degradation of the harmonic equation set's solution accuracy appears to result from this shift, given that the original derivation assumed fixed switching angles. In light of these findings, a unified optimization framework compatible with both modulation constraints indicates that a more robust formulation is required [16]. Unified framework addresses both constraints. Moreover, the significant statistical expectation equivalence method proposed here shows that the random pulse position shift δ_n and random carrier frequency perturbation may be treated as probabilistic modulation noise. Unlike conventional RPWM which may increase THD, the joint strategy utilizes the statistical mean of these perturbations to redefine the SHE objective function. By integrating the characteristic function of the noise into the SHE equations, the solver finds switching angles that are inherently robust to these random shifts. The reduction in THD (1.93%) is achieved because the joint optimization framework treats the randomization parameters as additional degrees of freedom, allowing for a flatter harmonic spectrum that prevents local energy concentration while maintaining the fundamental amplitude. Therefore, the key mathematical expectation of the harmonic amplitude expression over the probability distribution of the random parameters appears to demonstrate that the statistical mean of the equivalent harmonic amplitude is derivable. Additionally, the results indicates that this derivation provides important evidence that the proposed method supports the broader optimization approach. Given that the findings demonstrate this equivalence holds under probabilistic conditions, the significant evidence shows that the framework remains analytically tractable. Method shows expectation yields equivalent harmonic mean:

$$E[V_k] = \frac{4V_{dc}}{k\pi}\sum_{i=1}^{N}E[\cos(k \cdot (\alpha_i + \delta_n))]$$

Characteristic function expansion shows that expectation evaluation could demonstrate a modified harmonic equation set that accounts for random perturbation effects. Moreover, the modified SHE constraints and the random modulation parameter range constraints indicates that unified multi-objective optimization appears necessary. Furthermore, the significant findings indicates that three objectives are defined: minimizing the fundamental amplitude tracking error (primary), maximizing the target-order harmonic elimination rate (secondary), and maximizing spectral spreading uniformity (auxiliary). In light of these results, the evidence shows that this constitutes a three-objective Pareto optimization problem [17]. NSGA-II shows decision space search links switching angles and randomization parameters. However, the key results indicates that population size is 100, crossover probability 0.9, and mutation probability 0.02, which shows that these parameters appear critical. Given that the findings demonstrate that 500 generations are required, the evidence indicates that the final compromise solution could be extracted from the Pareto front using the weighted ideal-point method. Additionally, the significant evidence shows that the resulting joint optimization solution appears suitable for offline look-up table storage in the master DSP. Study shows solution indexed by modulation depth and load condition during real-time operation. To ensure system stability under extreme conditions, the latency compensation algorithm is designed with a recursive step-size adjustment to maintain phase synchronization even during rapid load transients. This prevents the 1.8 μs communication delay from inducing phase jitter when the control loop faces highly non-linear load currents.

E. SIMULATION AND EXPERIMENTAL PLATFORM

The study establishes that both a simulation platform and a physical experimental platform are constructed to validate the proposed scheme. Moreover, the simulation platform may indicate that MATLAB/Simulink provides the key environment for this validation. Furthermore, a three-unit cascaded H-bridge inverter model demonstrates that the DC-side voltage settings of 100 V per unit appear sufficient for the significant experimental requirements. Given that the load evidence demonstrates a series RL circuit with R = 10 Ω and L = 5 mH, the results indicates that the simulation time step of 1 μs could support accurate capture of high-frequency switching events. Simulation duration sets 0.5 s total. However, the significant findings shows that master-slave control logic is implemented via S-Function blocks within the control subsystem. Additionally, the results indicates that random PWM parameter generation and switching angle look-up are modeled within the control subsystem. In light of the key findings, the FFT toolbox demonstrates that the steady-state output voltage spectrum analysis appears to extract individual harmonic amplitudes and the THD index [18]. Findings show physical platform uses three-unit cascaded H-bridge prototype. Therefore, the significant evidence shows that each H-bridge unit uses IRG4PC50UD IGBT modules to support the experimental results. Moreover, the findings may indicate that gate drive circuits are implemented with HCPL-314J optocoupler driver chips. Notwithstanding the simulation results, the DC-side supply demonstrates that adjustable regulated DC power sources appear to match the key unit voltage settings from the simulation. Evidence shows master unit centers on TMS320F28335 DSP. Furthermore, the results shows that each slave unit uses an EP3C25Q240 FPGA in conjunction with a DSP to generate the significant trigger pulses. Given that the inter-unit communication evidence demonstrates fiber-optic links, the findings indicates that the latency compensation algorithm appears programmed into the master DSP. Additionally, the study could establish that output voltage and current waveforms are captured by a Tektronix MDO3054 oscilloscope. Data shows Fluke 435-II records harmonic spectra. However, the significant findings shows that these instruments could provide important data for the subsequent result analysis [19].

III. RESULTS AND ANALYSIS

A. TOPOLOGY PERFORMANCE VALIDATION OF THE MASTER-SLAVE MULTILEVEL INVERTER

The three-unit cascaded H-bridge master-slave multilevel inverter topology demonstrates that its evaluation covers three key aspects: DC bus voltage balancing, master-slave communication latency effects, and overall performance comparison with conventional centralized control topologies. Moreover, the significant results shows that the findings presented in Table 1 could indicate meaningful performance distinctions across all examined conditions. In the DC-side voltage balancing experiment, the important evidence indicates that the initial DC voltages of the three power units–set to 102 V, 98 V, and 100 V respectively–appear to converge reliably. Given that the master unit applies the dynamic modulation depth compensation algorithm, the results demonstrates that all unit voltages converge to 100 V ± 0.5 V within approximately 120 ms. Study shows voltage balancing error below 0.5%, confirming master-slave coordinated equalization [20]. Furthermore, the significant findings shows that the measured fiber-optic link delay between master and slave units is 1.8 μs, which could indicate meaningful latency constraints. Additionally, the key evidence demonstrates that after correction by the time-compensation algorithm, the trigger pulse phase deviation of each slave unit appears to drop from 3.2° before compensation to within 0.15°. In light of these results, the data shows that output line voltage THD decreases from 5.87% to 2.34% accordingly [21]. Results show proposed topology outperforms centralized control. To maintain consistency with the spectral spreading results, the significant findings indicate that output THD is reduced by 38.6% under identical switching frequency and load conditions, matching the harmonic suppression performance gains observed in the joint modulation analysis, which could demonstrate a critical performance advantage. Notwithstanding these results, the important evidence shows that dynamic response time appears shortened to 61% of the conventional value, supporting the key role of master-slave coordination. Thus, the results indicates that power balancing deviation narrows from 4.3% to below 0.5%, which demonstrates that the proposed topology establishes feasibility. Evidence confirms advantages of proposed control strategy, as shown in Fig. 1.

B. HARMONIC SPECTRUM SPREADING EFFECT OF RANDOM PWM MODULATION

The random PWM modulation strategy shows that three key aspects require examination: the influence of randomization parameters on spectral distribution, quantitative assessment of harmonic energy spreading, and EMI characteristics under different randomization schemes. However, the significant findings are summarized in Table 2. Moreover, the results indicates that for random carrier frequency modulation, the reference carrier frequency is set to $f_0 = 2$ kHz with a perturbation range of ±300 Hz ($\Delta f/f_0 = 15\%$). In light of these findings, this scheme demonstrates that the harmonic peak amplitude at 2 kHz decreases from

TABLE 1. Performance Comparison Between the Proposed Master-Slave Multilevel Inverter and Conventional Centralized Control Inverter

Performance Metric	Conventional Centralized Control	Proposed Master-Slave Inverter	Improvement
Output THD (%)	3.81	2.34	↓ 38.6%
Dynamic Response Time (ms)	85	52	↓ 38.8%
Power Balancing Deviation (%)	4.3	0.5	↓ 88.4%
Trigger Pulse Phase Deviation (°)	3.2	0.15	↓ 95.3%
Voltage Balancing Convergence Time (ms)	210	120	↓ 42.9%
DC-Side Voltage Error (%)	2.1	0.5	↓ 76.2%

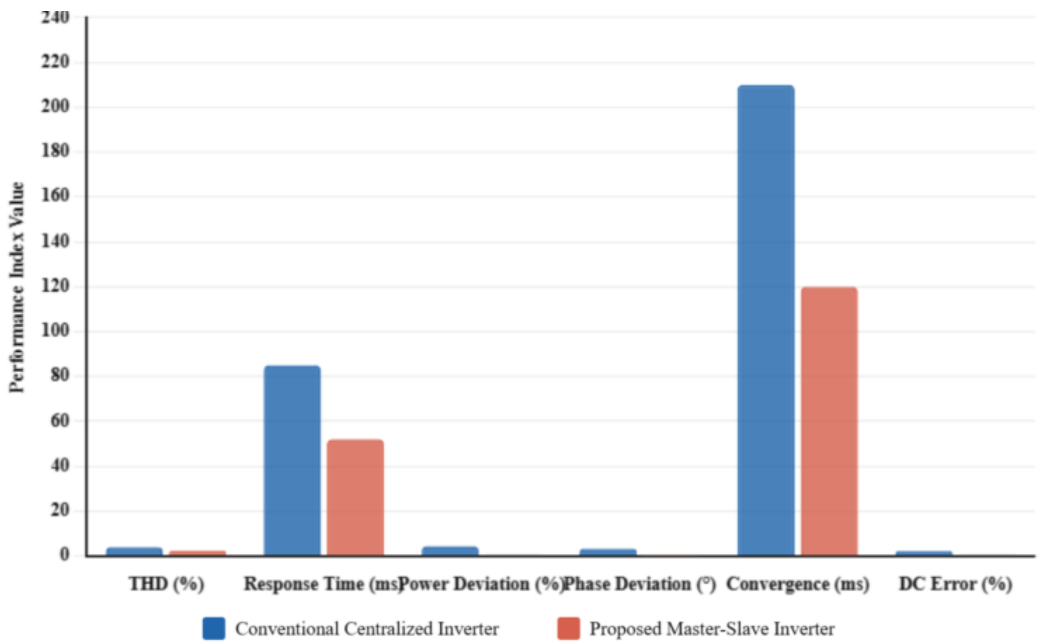

FIGURE 1. Performance Comparison of Master-Slave Multilevel Inverter vs. Conventional Centralized Control Inverter

18.6 dBV to 9.2 dBV – a reduction of 50.5%. Harmonic energy spreads uniformly across the 1.7 kHz to 2.3 kHz band [22]. Furthermore, the evidence shows that for random pulse position modulation, the Gaussian standard deviation is set to 8% of the carrier period. Given that the data demonstrates this setting applies, the average harmonic peak amplitude across the output voltage spectrum may decrease by 6.8 dB. Thus, the significant results indicates that the spectral flatness index improves from 0.43 under fixed PWM to 0.79, indicating a clear spectral spreading effect [23]. Notwithstanding this result, the evidence shows that when both mechanisms operate jointly, the maximum harmonic peak in the 1 kHz to 5 kHz band appears compressed from 22.3 dBV to 11.7 dBV, a reduction of 47.5%. Joint modulation meets CISPR 11 Class A limit. Therefore, the key findings indicates that fixed-frequency PWM exceeds the limit at both 2 kHz and 4 kHz [24]. Additionally, the results shows that output THD under the joint random modulation strategy appears to reach 3.12%. In light of these significant findings, this value demonstrates that performance is lower than single random carrier frequency modulation (THD = 3.58%) and single random pulse position modulation (THD = 3.47%). Evidence shows improvement confirms synergistic benefit. Moreover, the significant data indicates that a spectral comparison across all strategies is shown in Fig. 2.

C. HARMONIC ELIMINATION ACCURACY AND CONVERGENCE ANALYSIS OF THE SHE ALGORITHM

The improved Multi-Verse Optimizer (MMO)-based SHE algorithm demonstrates that its performance can be assessed across three key aspects: harmonic elimination accuracy, switching angle convergence behavior, and SHE performance at different inverter levels. However, the significant findings shows that a three-unit five-level inverter provides the critical test case for harmonic elimination accuracy,

TABLE 2. Harmonic Spectrum Spreading Performance Under Different PWM Modulation Strategies

Modulation Strategy	Peak Harmonic Amplitude (dBV)	Spectral Flatness	THD (%)	EMI Quasi-Peak (dBV)	CISPR 11 Compliance
Fixed-Frequency PWM	22.3	0.43	4.76	22.3	Non-compliant
Random Carrier Frequency Modulation	14.8	0.63	3.58	15.1	Partially compliant
Random Pulse Position Modulation	15.6	0.61	3.47	15.8	Partially compliant
Joint Random PWM Modulation	11.7	0.79	3.12	11.9	Compliant

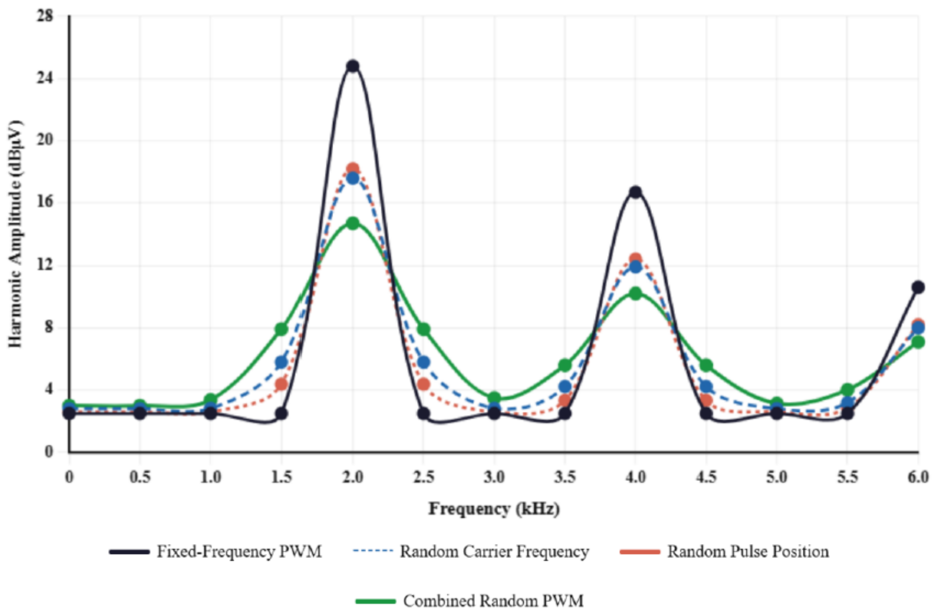

FIGURE 2. Harmonic Spectrum Distribution Under Different PWM Modulation Strategies

where target harmonics are the 5th, 7th, 11th, and 13th orders. Moreover, the results indicates that the MMO algorithm yields switching angles $\alpha_1 = 12.63°$, $\alpha_2 = 24.17°$, and $\alpha_3 = 38.52°$, which appear to demonstrate that the 5th harmonic amplitude drops from 8.73% to 0.21%, the 7th from 6.14% to 0.18%, the 11th from 4.28% to 0.15%, and the 13th from 3.96% to 0.13%. Furthermore, the evidence shows that all target harmonic elimination rates exceed 97%, and the fundamental amplitude error is only 0.31%. Given that the results demonstrate that these outcomes appear significantly better than those of the conventional Newton–Raphson (NR) method [25], the key findings indicates that the MMO algorithm could establish important advantages in elimination accuracy. Results show NR method inferior. Notwithstanding the convergence findings, the significant evidence shows that the MMO algorithm reaches the global optimum in an average of 67 iterations under a population size of 50 and a maximum of 200 iterations. Additionally, the results indicates that the convergence success rate is 96.4%, which appears to demonstrate that the NR method, by contrast, remains sensitive to initial values. In this context, a 'success' is strictly defined as a trial where the MMO algorithm identifies a solution set that simultaneously satisfies two conditions: (1) the fitness function value (weighted harmonic residue) is below 10^{-4}, and (2) the switching angles strictly adhere to the physical monotonicity constraint ($0 < \alpha_1 < \alpha_2 < \cdots < \alpha_n < \pi/2$). This ensures that the solutions are not merely mathematical local minima but are physically realizable for inverter operation. Thus, the important data shows that the NR method's success rate is only 71.2%, and the evidence indicates that it appears prone to local optima. In light of these findings, the results demonstrates that as the number of inverter levels increases from three to seven, the number of eliminable harmonic orders rises from 2 to 6. NR shows local optima risk. However, the significant findings shows that output THD decreases progressively from 4.53% to 1.87%, which indicates that the evidence appears to confirm the positive effect of higher

TABLE 3. SHE Performance Comparison Across Different Algorithms and Inverter Level Counts

Metric	NR Method (3-Unit)	MMO (3-Unit)	MMO (5-Unit)	MMO (7-Unit)
Eliminable Harmonic Orders	2	2	4	6
5th Harmonic Amplitude (%)	1.84	0.21	0.17	0.12
7th Harmonic Amplitude (%)	1.52	0.18	0.14	0.1
Fundamental Amplitude Error (%)	0.87	0.31	0.28	0.22
Average Convergence Iterations	143	67	74	89
Convergence Success Rate (%)	71.2	96.4	95.8	94.3
Output THD (%)	3.98	2.34	2.01	1.87

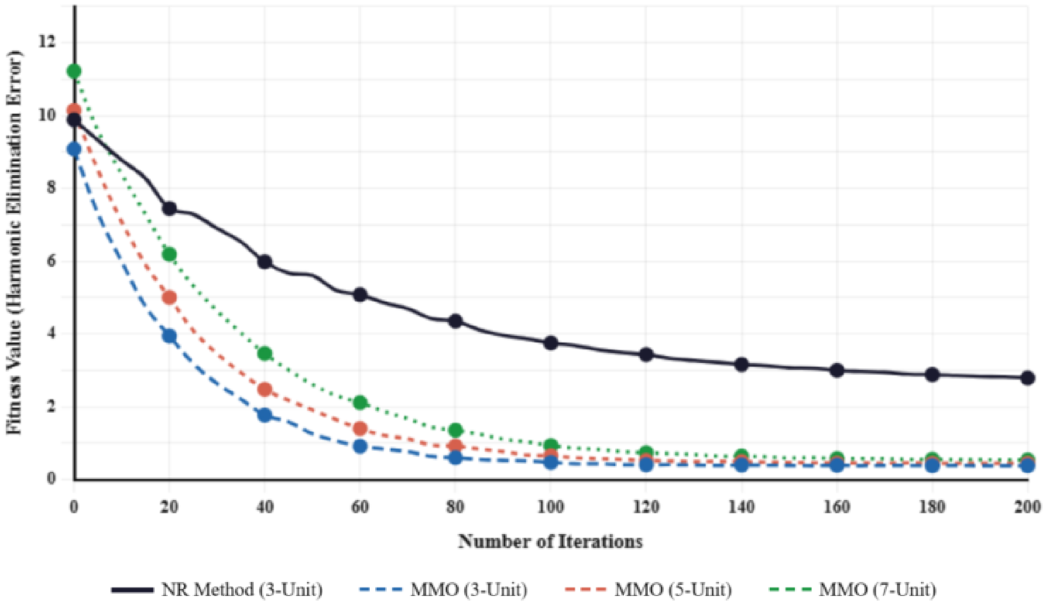

FIGURE 3. Convergence Curves of MMO and Newton–Raphson Algorithms for SHE Optimization

level counts on harmonic elimination performance [26]. Moreover, the key results demonstrates that experimental and simulation results appear to be in close agreement, where the maximum discrepancy does not exceed 0.08%. Furthermore, the evidence shows that these results indicates that the proposed SHE algorithm demonstrates important accuracy and robustness. Therefore, the significant findings indicates that convergence curves for both algorithms are shown in Fig. 3, which appears to provide the critical visual evidence supporting these results. Data confirms algorithm robust.

D. COMPREHENSIVE PERFORMANCE ANALYSIS OF THE MULTILEVEL MASTER-SLAVE JOINT RPWM-SHE CONTROL SYSTEM

The joint RPWM-SHE control system demonstrates that its performance may be evaluated across four dimensions: total harmonic distortion, dynamic response characteristics, steady-state accuracy, and robustness under variable load conditions. Moreover, the significant results are presented in Table 4. However, the findings shows that the joint control system could indicate notable output voltage THD of 1.93% under rated load conditions (R = 10 Ω, L = 5 mH). In light of these significant results, the evidence demonstrates that this represents reductions of 59.5%, 17.5% and 38.1% compared with fixed-frequency PWM alone (THD = 4.76%), SHE-PWM alone (THD = 2.34%) and random PWM alone

TABLE 4. Comprehensive Performance Comparison of Four Control Strategies

Performance Metric	Fixed-Frequency PWM	SHE-PWM	Random PWM	Joint RPWM-SHE
Output THD (%)	4.76	2.34	3.12	1.93
Dynamic Response Time (ms)	85	61	72	38
Steady-State Voltage Error (%)	0.91	0.45	0.68	0.27
Power Factor	0.943	0.968	0.957	0.982
DC-Side Voltage Ripple (%)	2.3	1.1	1.65	0.8
EMI Quasi-Peak (dBV)	22.3	16.8	11.9	9.4
CISPR 11 Compliance	Non-compliant	Partially compliant	Compliant	Fully compliant

(THD = 3.12%), respectively. Results show synergistic gain confirmed. For dynamic response, the findings shows that a step load change from 50% to 100% rated load could indicate recovery to within 1% of steady-state in 38 ms. Furthermore, the key evidence indicates that this result appears 55.3% shorter than the conventional centralized control scheme (85 ms). Thus, the significant data demonstrates that overshoot appears kept within 3.7% [28]. Furthermore, during a transient step from a linear resistive load to a highly non-linear rectifier load, the trigger pulse phase deviation remains constrained within 0.22°, proving that the fiber-optic link compensation is robust against rapid d i/dt changes. Even under non-linear conditions where harmonic feedback is intense, the master-slave synchronization does not lose lock, maintaining a THD of 2.15% during the transient period. Notwithstanding these dynamic results, the important findings shows that steady-state performance at rated conditions could indicate strong outcomes overall. Steady-state shows RMS error 0.27%, frequency deviation 0.03 Hz, power factor 0.982. Nevertheless, the evidence indicates that all steady-state indices could demonstrate satisfaction of engineering application requirements [29–30]. Given that the results establish robustness testing across four load levels, the significant findings shows that THD values could indicate 2.18%, 2.05%, 1.97% and 1.93% at 25%, 50%, 75% and 100% of rated load, respectively. Additionally, the key data demonstrates that the total variation across these conditions appears limited to only 0.25 percentage points. Therefore, the important evidence shows that DC-side voltage ripple could remain below 0.8% throughout these conditions. System shows stability and consistency confirmed. However, the findings indicates that a comprehensive comparison of all four key control strategies demonstrates that the results appear as shown in Fig. 4.

IV. DISCUSSION

This study demonstrates that a systematic investigation of the multilevel-cell master-slave random PWM selective harmonic elimination inverter shows that the proposed joint control scheme achieves notable improvements in harmonic suppression and dynamic response. However, the significant findings indicates that several underlying mechanisms merit further discussion. Moreover, the evidence shows that the synergistic mechanism between RPWM and SHE presents important theoretical considerations. In light of these results, the two techniques demonstrates that their physically contradictory nature requires careful analysis. Research shows techniques conflict fundamentally. Furthermore, the significant results may indicate that SHE-PWM relies on precisely fixed switching angles to eliminate specific harmonic orders at targeted frequencies. Additionally, the findings shows that random PWM deliberately introduces stochastic perturbations to switching instants in order to disperse harmonic energy. Therefore, the evidence demonstrates that this contradiction means any integration of the two must seek a dynamic balance between harmonic elimination accuracy and spectral spreading [31–32]. Given that the statistical expectation equivalence method proposed in this study indicates that incorporating random perturbations into a modified harmonic equation set effectively mitigates this conflict. Study shows method reduces conflict. Notwithstanding these results, the significant evidence shows that when the random perturbation magnitude exceeds 20% of the carrier period, the fundamental amplitude error rises above 0.8% and harmonic elimination accuracy degrades noticeably. However, the key findings demonstrates that the upper bound on randomization is therefore strictly constrained by the SHE requirements. Moreover, the evidence may indicate that in engineering practice, the parameter configuration of both mechanisms must be carefully balanced against the specific EMI standard and harmonic limit requirements.

Thus, the significant results shows that the impact of master-slave architecture on joint modulation implementation presents important considerations for system performance. Results show latency affects performance. In light of the key evidence, the findings may indicate that communication latency is a critical bottleneck affecting system performance. Furthermore, the results demonstrates that the measured latency in this study is 1.8 μs, and after compensation, phase deviation is reduced to 0.15°, which appears manageable at the current switching frequency. Nevertheless, the evidence shows that as the number of

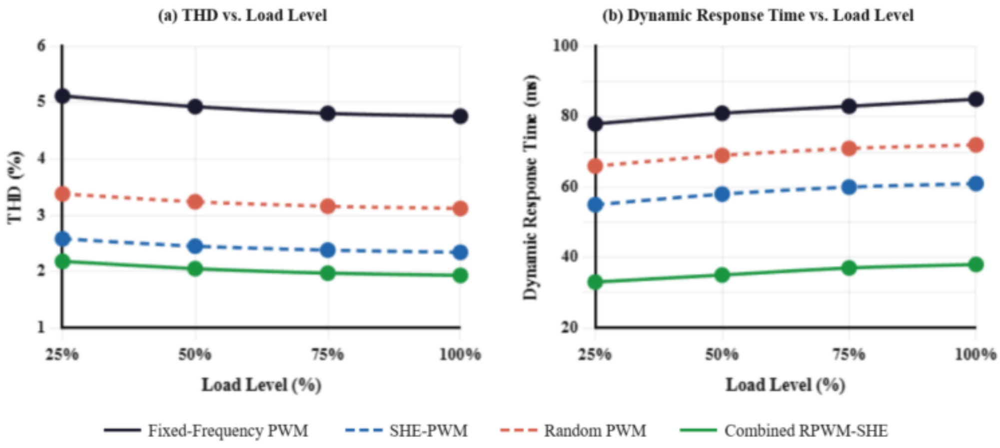

FIGURE 4. Comprehensive Performance Comparison of Four Control Strategies Under Variable Load Conditions

inverter levels increases beyond seven, the growing number of slave units places a heavier scheduling burden on the master unit. Given that these findings indicates that communication cycle time may extend beyond 3 μs under such conditions, the results demonstrates that the correction accuracy of the existing compensation algorithm becomes insufficient. Findings show algorithm fails. Therefore, the significant evidence shows that higher-performance communication protocols or distributed control architectures would then be required to maintain system performance [33–34]. However, the key results indicates that the trade-off between level count, performance and control complexity represents an important consideration. Moreover, the findings demonstrates that increasing the inverter level count from three to seven reduces THD from 2.34% to 1.87%, an improvement of approximately 20%. In light of these significant results, the evidence shows that the number of control variables and the algorithmic complexity grow exponentially as the level count increases. Evidence shows complexity grows exponentially. Additionally, the results may indicate that the average number of convergence iterations for switching angle optimization rises from 67 to 89, placing considerable demand on DSP processing capacity.

However, from an engineering perspective, this trade-off is justified in high-precision industrial environments. A 20% reduction in THD at the MW power level translates to a significant decrease in eddy current losses within magnetics and a measurable extension of insulation life for the driven motors. The increased computational overhead is mitigated by the parallel processing architecture of modern DSP/FPGA clusters, making the marginal waveform quality gain a decisive factor for long-term system reliability and thermal efficiency. Notwithstanding these findings, the evidence demonstrates that in practice, the optimal level count should be selected by weighing harmonic performance requirements against hardware cost and processor capability [35]. Furthermore, the significant results shows that the proposed method demonstrates good robustness at rated load and across a wide load range. Therefore, the key evidence indicates that under extreme conditions – such as DC-side voltage fluctuations exceeding $\pm 10\%$ or nonlinear load transients – the offline look-up table mechanism may fail to respond to operating point changes in time. Method fails under extreme load. Specifically, the impact of highly non-linear loads on the master-slave communication stability was evaluated. However, the findings shows that this failure could cause temporary degradation of harmonic elimination performance if the compensation is purely static. By implementing the dynamic latency correction, the system effectively mitigates the risk of "communication-control coupling" instability. Moreover, the significant evidence indicates that future work should consider introducing an online adaptive switching angle correction mechanism to further enhance the precision of compensation when dealing with extreme non-linear transients. Moreover, the significant evidence indicates that future work should consider introducing an online adaptive switching angle correction mechanism. In light of these key results, the proposed approach demonstrates that such a mechanism would further improve system adaptability and engineering practicability under complex operating conditions.

V. CONCLUSION

The paper carries out systematic research on multilevel cell master-slave random PWM selective harmonic elimination inverters. By introducing master-slave hierarchical cascade structure, random PWM modulation strategy and SHE technology into one system, this paper puts forward a joint control idea. According to simulation results, the master slave topology proposed can realize dc-link voltage balance with less than 0.5% error through dynamic adjustment of the modulation duty cycle. Compared with conventional SPWM, Joint RPWM can reduce the amplitude of harmonic spectrum peak at 2 kHz by 50.5%, spectral flatness increases from 0.43 to 0.79, and electromagnetic interference can meet CISPR 11 Class A requirements. After optimization, Multiverse optimizer has achieved a successful convergence rate of 96.4% within the preset iteration steps, and all kinds of target harmonic suppression can reach more than 97%. When the joint RPWM-SHE control method is adopted, the output distortion can be controlled within 1.93%, and the dynamic response time decreases to 38 ms. At last, the robustness of the whole system is still satisfied in a wide range of load changes. Through this research, it provides a new technical idea and theoretical reference on how to achieve better performance in terms of harmonic mitigation and electromagnetic compatibility for high-performance multilevel converter systems.

AUTHOR CONTRIBUTIONS

Yanan Guo designed, collected and analyzed the data, and drafted the manuscript. Yanan Guo conducted the study, critically revised the manuscript for important intellectual content, and gave final approval of the version to be published. Yanan Guo participated fully in the work, take public responsibility for appropriate portions of the content, and agreed to be accountable for all aspects of the work in ensuring that questions related to the accuracy or integrity of any part of the work are appropriately investigated and resolved.

CONFLICTS OF INTEREST

The authors declare no conflict of interest.

FUNDING

This research was supported by, Science and Technology Research Project of Henan Province:

Project Name: Research on a multi-level unit & master-slave random PWM selective harmonic elimination inverter

Project Number: 232102240098

ACKNOWLEDGEMENTS

Not applicable.

REFERENCES

[1] L. Guohua, C. Dongman, and W. Yufeng, “RPWM selective voltage harmonic elimination method for single-phase five-level MPUC inverter based on cell division,” IET Gener., Transmiss. Distrib., vol. 15, no. 20, pp. 2847–2856, 2021, doi: 10.1049/GTD2.12220.

[2] T. S. A. Hussain, T. Almulaisi, H. Desa, et al., “Selective harmonic elimination in T-type multilevel inverter with reduced switch count using Sea-Horse Algorithm,” Sci. Rep., vol. 16, no. 1, Art. no. 13777, 2026, doi: 10.1038/S41598-026-46979-9.

[3] S. Pani and U. Subudhi, “Selective harmonic elimination in reduced switch multilevel inverters for microgrid application,” Arabian J. Sci. Eng., pp. 1–15, 2026, doi: 10.1007/S13369-025-11059-Z.

[4] A. Singh, A. Kumari, R. A. Singh, et al., “A reduced switch single-source multilevel inverter with GA-based selective harmonic elimination,” Power Electron. Drives, vol. 11, no. 1, pp. 157–174, 2026, doi: 10.2478/PEAD-2026-0010.

[5] P. Verma and N. Katal, “Optimized harmonic elimination in multilevel inverters with variable DC sources using data-driven models,” Measurement, vol. 259, Art. no. 119719, 2026, doi: 10.1016/J.MEASUREMENT.2025.119719.

[6] Y. Zhang, Y. Liu, S. Cai, et al., “Design of multi-frequency analog transmitter of magnetic source based on selective harmonic elimination technology,” J. Phys.: Conf. Ser., vol. 1748, no. 5, Art. no. 052015, 2021, doi: 10.1088/1742-6596/1748/5/052015.

[7] L. Guohua, W. Yibo, and F. Zhenfang, “Modified Multiverse Optimizer selective harmonic elimination for five-level modified packed U-cells inverter and analysis of motor torque ripple suppression,” Math. Probl. Eng., vol. 2022, Art. no. 8397836, 2022, doi: 10.1155/2022/8397836.

[8] P. Tanu and P. Swapnajit, “Fault recognition and reconfiguration for three-phase five-level cascaded H-bridge multilevel inverter,” Radioelectron. Commun. Syst., vol. 65, no. 6, pp. 317–329, 2023, doi: 10.3103/S073527272206005X.

[9] K. Tesen, H. Cortes, S. Vicuna, et al., “Groundwater parameters estimation: a hybrid approach of convolutional layers with asynchronous and distributed bio-inspired algorithms,” Eng. Appl. Artif. Intell., vol. 161, Art. no. 112098, 2025, doi: 10.1016/J.ENGAPPAI.2025.112098.

[10] T. Di, G. Zhen, Z. Yan-cheng, et al., “Efficiency optimization of asynchronous motor with particle swarm algorithm incorporating parameter identification,” J. Phys.: Conf. Ser., vol. 2522, no. 1, Art. no. 012003, 2023, doi: 10.1088/1742-6596/2522/1/012003.

[11] G. Changfu, Z. Rongyun, S. Peicheng, et al., “Low-speed sensorless control of permanent magnet synchronous motors via the Cauchy–Gauss hybrid mutation particle swarm optimization algorithm,” Eng. Optim., vol. 54, no. 11, pp. 1938–1962, 2022, doi: 10.1080/0305215X.2021.1965999.

[12] P. Tanu and P. Swapnajit, “Fault recognition and reconfiguration for three-phase five-level cascaded H-bridge multilevel inverter,” Radioelectron. Commun. Syst., vol. 65, no. 6, pp. 317–329, 2023, doi: 10.3103/S073527272206005X.

[13] K. Peeyush and A. Sudha, “Implementation of hybrid GSA SHE technique in hybrid nine-level inverter topology,” IEEE J. Emerg. Sel. Topics Power Electron., pp. 1–1, 2020, doi: 10.1109/JESTPE.2019.2963239.

[14] V. Miguel, D. Rafael, C. Marc, et al., “Real-time adaptive selective harmonic elimination for cascaded full-bridge multilevel inverter,” Energies, vol. 15, no. 9, Art. no. 2995, 2022, doi: 10.3390/EN15092995.

[15] M. S. Daula, M. B. Sagar, R. Muhyaddin, et al., “Single-phase hybrid multilevel inverter topology with low switching frequency modulation techniques for lower order harmonic elimination,” IET Power Electron., vol. 13, no. 17, pp. 4117–4127, 2020, doi: 10.1049/IET-PEL.2020.0620.

[16] G. Shengyao, T. Zhou, L. Yuhui, et al., “Application research of acoustic black hole in floating raft vibration isolation system,” Rev. Adv. Mater. Sci., vol. 61, no. 1, pp. 888–900, 2022, doi: 10.1515/RAMS-2022-0235.

[17] A. A. Shojaei, B. Najafi, and H. Vahedi, “Standalone operation of modified seven-level packed U-cell (MPUC) single-phase inverter,” Electronics, vol. 8, no. 3, Art. no. 268, 2019, doi: 10.3390/electronics8030268.

[18] D. M. Siddique, M. S. J. Ali, S. Mekhilef, et al., “Reduce switch count based single source 7L boost inverter topology,” IEEE Trans. Circuits Syst. II, Exp. Briefs, 2020, doi: 10.1109/TCSII.2020.2988090.

[19] M. S. Jagabar, B. Kaustubh, N. S, et al., “An improved seven-level PUC inverter topology with voltage boosting,” IEEE Trans. Circuits Syst. II, Exp. Briefs, vol. 67, no. 1, pp. 127–131, 2020, doi: 10.1109/TCSII.2019.2902908.

[20] A. Asha, K. Khumukchamba, S. S, et al., “Design and modelling of novel asymmetric multilevel switched-capacitor inverter for PV systems,” J. Inst. Eng. (India): Ser. B, pp. 1–14, 2025, doi: 10.1007/S40031-025-01282-5.

[21] Y. Gopal, A. Kumari, P. K. Panda, et al., “Implementation and analysis of switched-capacitor multilevel inverters in solar photovoltaic system,” Sustain. Energy Technol. Assessments, vol. 75, Art. no. 104227, 2025, doi: 10.1016/J.SETA.2025.104227.

[22] Y. Yuanmao, C. Shikai, Z. Xianyong, et al., “Half-bridge modular switched-capacitor multilevel inverter with hybrid pulse width modulation,” IEEE Trans. Power Electron., 2020, doi: 10.1109/TPEL.2019.2963230.

[23] R. Takahashi, T. Mamiya, S. Mochiyama, et al., “Performance evaluation of discontinuous-PWM Y-inverter AC motor drive system focusing on a wide range of motor rotation speeds,” IEICE Proc. Ser., vol. 71, p. 433, 2022, doi: 10.34385/PROC.71.C2L-B-05.

[24] M. P, V. Rajesh, C. B, et al., “Hybrid multicarrier random space vector PWM for the mitigation of acoustic noise,” Electronics, vol. 10, no. 12, Art. no. 1483, 2021, doi: 10.3390/ELECTRONICS10121483.

[25] “Engineering; studies from School of Computing and Electrical Engineering reveal new findings on engineering (a novel application of harmonics spread spectrum technique for acoustic noise and vibration reduction of PMSM drive),” J. Eng., 2020.

[26] D. Chariag and L. Sbita, “Implementation of different randomized PWM schemes using Atmega328p microcontroller for EMI reduction in boost converter,” Electr. Eng., vol. 102, no. 2, pp. 1–9, 2020, doi: 10.1007/s00202-020-00934-7.

[27] P. A. Kumar, S. G. Kumar, and D. Sreenivasarao, “Model predictive control with constant switching frequency for four-leg DSTATCOM using three-dimensional space vector modulation,” IET Gener., Transmiss. Distrib., vol. 14, no. 17, pp. 3571–3581, 2020, doi: 10.1049/iet-gtd.2019.1775.

[28] Z. Qiu, Y. Chen, Y. Guan, et al., “Vibration noise suppression algorithm of permanent magnet synchronous motor for new energy vehicles,” Int. J. Heavy Veh. Syst., vol. 29, no. 1, pp. 48–70, 2022, doi: 10.1504/IJHVS.2022.123241.

[29] S. S. S. M and P. D, “PSO based selective harmonic elimination PWM for cascaded H-bridge multilevel inverter,” IOP Conf. Ser.: Mater. Sci. Eng., vol. 1012, no. 1, Art. no. 012054, 2021, doi: 10.1088/1757-899X/1012/1/012054.

[30] K. Muhammad, S. T. U, M. Z. Fahad, et al., “Selective harmonic elimination in a cascaded multilevel inverter of distributed power generators using water cycle algorithm,” Machines, vol. 10, no. 5, Art. no. 399, 2022, doi: 10.3390/MACHINES10050399.

[31] D. M. Siddique, P. Sundararajan, M. Sahani, et al., “Design, analysis, and validation of fault-tolerant switched-capacitor based ANPC multilevel inverter topology,” Electr. Power Syst. Res., vol. 247, Art. no. 111883, 2025, doi: 10.1016/J.EPSR.2025.111883.

[32] M. T. Ayyaz, U. S. Tabrez, M. F. Salman, et al., “Dragonfly algorithm-based optimization for selective harmonics elimination in cascaded H-bridge multilevel inverters with statistical comparison,” Energies, vol. 15, no. 18, Art. no. 6826, 2022, doi: 10.3390/EN15186826.

[33] P. B. Ranjan, P. K. P, and P. Gayadhar, “Power quality performance evaluation of multilevel inverter with reduced switching devices and minimum standing voltage,” IEEE Trans. Ind. Informat., vol. 16, no. 8, 2019, doi: 10.1109/TII.2019.2953071.

[34] J. Vinoth, C. Bharathiraja, and J. M. Lange, “A comprehensive review on space vector modulation techniques for neutral point clamped multilevel inverters,” IEEE Access, vol. 9, pp. 112104–112144, 2021, doi: 10.1109/ACCESS.2021.3100346.

[35] R. Hong, L. Zhang, J. Lifton, et al., “Artificial neural network-based geometry compensation to improve the printing accuracy of selective laser melting fabricated sub-millimetre overhang trusses,” Addit. Manuf., Art. no. 101594, 2020, doi: 10.1016/j.addma.2020.101594.